J. Cent. South Univ. (2015) 22: 1087−1095
DOI: 10.1007/s11771-015-2620-9

Springer

Effect of strain rate and water-to-cement ratio on compressive mechanical behavior of cement mortar

ZHOU Ji-kai(周继凯), GE Li-mei(葛利梅)

College of Civil and Transportation Engineering, Hohai University, Nanjing 210098, China

© Central South University Press and Springer-Verlag Berlin Heidelberg 2015

Abstract: Effects of strain rate and water-to-cement ratio on the dynamic compressive mechanical behavior of cement mortar are investigated by split Hopkinson pressure bar (SHPB) tests. 124 specimens are subjected to dynamic uniaxial compressive loadings. Strain rate sensitivity of the materials is measured in terms of failure modes, stress−strain curves, compressive strength, dynamic increase factor (DIF) and critical strain at peak stress. A significant change in the stress−strain response of the materials with each order of magnitude increase in strain rate is clearly seen from test results. The slope of the stress−strain curve after peak value for low water-to-cement ratio is steeper than that of high water-to-cement ratio mortar. The compressive strength increases with increasing strain rate. With increase in strain rate, the dynamic increase factor (DIF) increases. However, this increase in DIF with increase in strain rate does not appear to be a function of the water-to-cement ratio. The critical compressive strain increases with the strain rate.

Key words: cement mortar; loading rate; compressive strength; critical strain; stress−strain behavior

1 Introduction

Terrorist attacks, explosion scenarios in tunnels and the potential hazards from storage of high energetic materials have become important safety issues. Concrete is the most widely used manufactured material in the world. In particular, it is employed in the building of highly sensitive infrastructure (civil engineering structures, dams, nuclear power plants, and etc). Knowledge about the response of concrete structures to impact and explosive loading is required for reliable safety assessment and the design of protective structures [1]. A complicating factor is the fact that cement-based materials are rate-dependent materials [2], which means that the mechanical properties of concrete depend on the applied loading rate. The mechanical response of structures exposed to explosive loading can only be predicted properly with material models that include this rate effect.

The strain-rate sensitive behavior of concrete and its constituents have been under investigation for several decades [3]. In most studies, the compressive strength of concrete has been observed to increase approximately linearly with each order of magnitude (factor of 10) increase in strain rate, up to moderate strain rates, e.g., about 10^0 s^{-1} [4−6]. Generally, the increase has been 7% to 15% with each order of magnitude increase in strain rate [3]. In a few cases, however, the increase has been considerably less [7] or insignificant [8]. At high strain rates (i.e. above 10^0 s^{-1}), there has been less agreement among various studies. Some have observed that the linear relation is maintained up to strain rates as high as 800 s^{-1} [9−10], while others have found the relation to either being concave upward [11], or concave downward [12] with increasing strain rate.

Knowledge of high strain rate behavior of concrete is rather limited, with emphasis placed mainly to observe strength increases and little attention paid to changes in deformation behavior. The critical strain at the maximum strength or peak stress is an important parameter in the characterization of material behavior. There have been differing interpretations regarding how this strain varies with the strain rate [3].

In this investigation, an experimental study on the influence of strain rate and water-to-cement ratio on compressive mechanical behavior of cement mortar was carried out. A split Hopkinson pressure bar (SHPB) system was used in this work.

2 Experiment

2.1 Materials and specimens

Ordinary Portland cement (OPC) was used in the production of cement mortar specimens. The cement was the most widely used cement in general concrete

Foundation item: Project(51479048) supported by National Natural Science Foundation of China
Received date: 2013−11−20; **Accepted date:** 2014−03−31
Corresponding author: ZHOU Ji-kai, Professor, PhD; Tel: +86−13601469968; E-mail: zhoujikaihhu@163.com

construction works in China. The fine aggregate was river sand consisting mainly of quartz, with 10% feldspar. The gradation test showed that the particle size of the sand was continuously distributed within the range of 0.4−2.5 mm with 80% of sand. Three water-to-cement ratios (*w*/*c*), 0.3, 0.4, and 0.5, were used for cement mortar. The sand-to-cement ratio for all cement mortar was 2.

The standard specimens were cast in steel molds with dimensions of 150 mm×150 mm×550 mm. Following casting, the specimens were covered with a plastic membrane to prevent the moisture from evaporating. The specimens were de-moulded after 24 h, and then moist-cured in a water tank at 20 °C. After curing for 90 d, the specimens were cored from the standard specimens. Mortar cores were cut and ground smoothly to produce 37-mm-diameter cylindrical specimens of 18.5 mm in thickness for the quasi-static and split Hopkinson pressure bar test. 124 specimens were made for the dynamic tests. Also, several companion specimens of 37 mm×37 mm×74 mm were prepared for obtaining static compressive strength of cement mortar. For static compressive tests, the length to diameter ration had to be 2 or more to minimize the end effect. The following values were obtained for the cement mortar at the age of 90 d: compressive strengths of 49.59 MPa, 38.43 MPa, and 31.50 MPa for *w*/*c*=0.3, 0.4, and 0.5, respectively.

2.2 Split Hopkinson pressure bar tests

The dynamic compression tests were performed using a SHPB which is a very popular experimental approach for studying the dynamic responses of materials at high strain rates. Figure 1 shows the schematic of the SHPB system used in this work.

The SHPB system consists of a gas gun chamber, a striker bar, an incident bar and a transmission bar. The strain gauges are permanently mounted on the system at the middle of the incident bar and the transmitted bar. When the striker bar hits the ends of the incident bar, an elastic compression stress pulse is generated. The shape of this pulse in stress−time coordinates is almost rectangular, and the amplitude is promotional to the impact velocity of the striker bar. This pulse propagates towards the specimen. When the incident pulse reaches the interface of the incident bar and specimen, a portion of the pulse is reflected back along the input bar as tensile pulse and the remaining portion is transmitted into the specimen as a compressive wave toward the transmission bar [13]. The strain gauge is mounted on the input bar and the output bar to record the pulse signals. In all dynamic testing processes, the strain signal is recorded using a digital oscilloscope.

The specimens are placed between the two long horizontally aligned pressure bars served as the medium for the propagation of elastic pulses as well as for measuring the stress−time history. All three waves, i.e., an incident compressive pulse generated by the impact of a striker, a reflected tensile pulse due to the low impedance of the specimen and a transmitted compressive wave, are measured at the gauge locations, situated at some distance away from the interface. Therefore, an appropriate time shifting procedure must be undertaken to transfer the strain histories from the gauge locations to the interfaces.

Assuming that axial wave propagation and homogeneous stress distribution in the specimen, the resulting stress $\sigma_s(t)$, strain $\varepsilon_s(t)$ and strain rate $\dot{\varepsilon}$ of the specimen are obtained by the following equations [14]:

$$\sigma_s(t) = E_b\left(\frac{A_b}{A_s}\right)\varepsilon_T(t) \tag{1}$$

$$\varepsilon_s(t) = -\frac{2C_0}{l}\int_0^t \varepsilon_R(t)\,\mathrm{d}t \tag{2}$$

$$\dot{\varepsilon} = \frac{\mathrm{d}\,\varepsilon_s(t)}{\mathrm{d}\,t} \tag{3}$$

where A_b, E_b and C_0 are the cross-sectional area, the elastic modulus and the wave velocity of the bar material, respectively; l, A_s are the length and cross-sectional areas of the specimen, respectively.

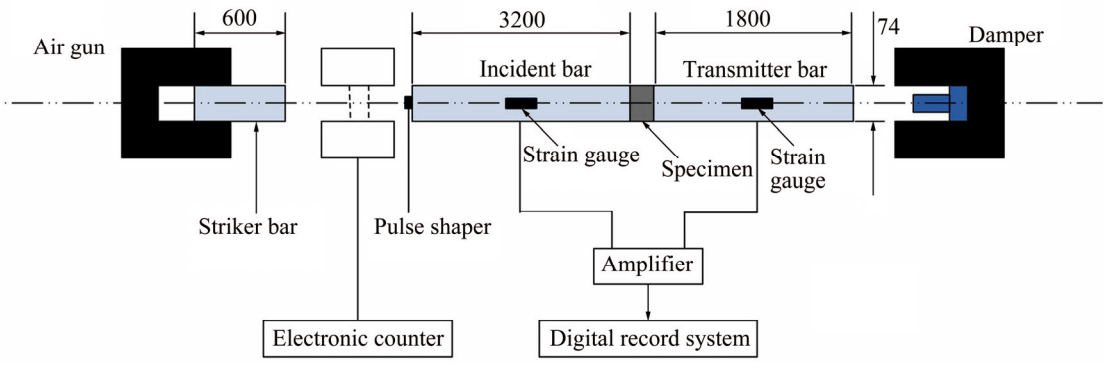

Fig. 1 Schematic of split Hopkinson pressure bar (SHPB) (Unit: mm)

The pulse shaping technique in SHPB is especially useful for investigating the dynamic response of brittle materials, such as rocks and concrete [15]. During the dynamic tensile tests, the striker impact on the pulse shaper before the incident bar, generates a non-dispersive ramp pulse propagating into the incident bar and thus facilitates the dynamic force balance for the specimen. Then, the dynamic force balance on the two ends of the sample is critically assessed. In this investigation, the pulse shaper is made up of a thin copper disc (with 0.9 mm in diameter and 0.8 mm in thickness).

3 Test results and discussion

3.1 Failure mode

It can be seen from the test results that, as the strain rate increased, specimens failed with an increasing number of cracks and fragments. At a low strain rate, the specimens may fail without fracturing and the failure occurs when multiple cracks become connected and run through the specimen. At a high strain rate, mortar specimens generated particles of sand and paste in the failure regions. The failure cracks in low water-cement ratio specimens were generally straighter, longer and cleaner than the cracks in high water-to-cement ratio specimens. Mortar specimens, especially those with high water-to-cement ratios, failed with comparatively less violence.

In mortar specimens, as a crack grows under increasing strain, it eventually meets a relatively stiffer sand particle and is arrested, at least temporarily. If the applied strain rate is slow enough, the crack eventually grows around the in-homogeneity. However, at higher strain rates, more and more such cracks find insufficient time to grow around the stiff in-homogeneities. At high strain rates, two alternative processes are likely for each growing crack: 1) the crack is forced to grow through a stiffer zone, or 2) the increased local stress intensity is relieved by the initiation or growth of other cracks in the vicinity that have no hindrances. The former process causes more violent failure mode. These processes are intensified as the *w/c* is lowered, namely. the number of un-hydrated particles is increased, and making mortar specimens with the lowest water-to-cement ratio (0.3) fail most violently.

3.2 Stress−strain curves

Figures 2 to 4 show stress−strain curves at different strain rates for specimens with different *w*/*c* (0.3, 0.4 and 0.5), respectively. A significant change in the stress−strain response of the materials with each order of magnitude increase in strain rate is clearly seen in these figures. For each specimen, as the strain rate is increased, both the initial slope and the peak stress increase, while the nonlinearity of the initial response decreases. During rapid impact loading the slope of the curves has also been observed to remain linear up to higher stress levels, indicating a delay in the internal cracking process. The slope of the stress−strain curve after peak value for low water-to-cement ratio is steeper than that of high water-to-cement ratio mortar. This indicates that the fracture behavior of low water-to-cement ratio mortar is more brittle than high water-to-cement ratio mortar.

For mortar specimens, the sand particle−matrix transition zone is very weak compared with both the matrix and sand particles. In addition, these transition zones contain preexisting flaws created by bleed water that has collected below the sand particles. The growing cracks, even at high strain rates, find enough weak links, in the form of the preexisting flaws at the sand−matrix interface, to grow without being forced through the stiffer and particles.

As motioned in section 3.1, the stiffer sand particles raise local stress intensities, as well as provide weak zones for the preexisting flaws to grow into cracks. At high strain rates, the presence of in-homogeneities, both sand and matrix, does provide for some crack arrest, causing both the peak stress and the strain at the peak stress to increase. The smallest increase in relative ductility with increasing strain rate occurs in the case of mortar specimens with the highest water-to-cement ratio (0.5). This is expected since these mortars have the highest density of flaws due to bleed water.

As the strain rate increased, the compressive strength (i.e. peak stress) and the strain at the peak stress both increase. Others have observed similar variations for concrete materials [3]. Special aspects of the response of the materials as a function of strain rate and water-to-cement ratio are discussed next.

3.3 Dynamic compressive strength

Figure 5 shows the dynamic compressive strength (δ) of all specimens (*w*/*c*=0.3, 0.4 and 0.5). Significant strength increase with increase in strain rate is observed in all water-to-cement ratios. The results also indicate that dynamic compressive strength is dependent on the water-to-cement ratio of the mix.

The present strength in this investigation was analyzed to formulate statistical models relating dynamic compressive strength with strain rates and water-to-cement ratio. As early as 1918, a systematic method of formulating concrete mixtures was published by FREW et al [16]. He enunciated the relationship between water-to-cement ratio and strength as follows: For a given set of materials, the strength development depends only on one factor, i.e., the ratio of water to cement content in a given mix, with the functional relation being expressed as

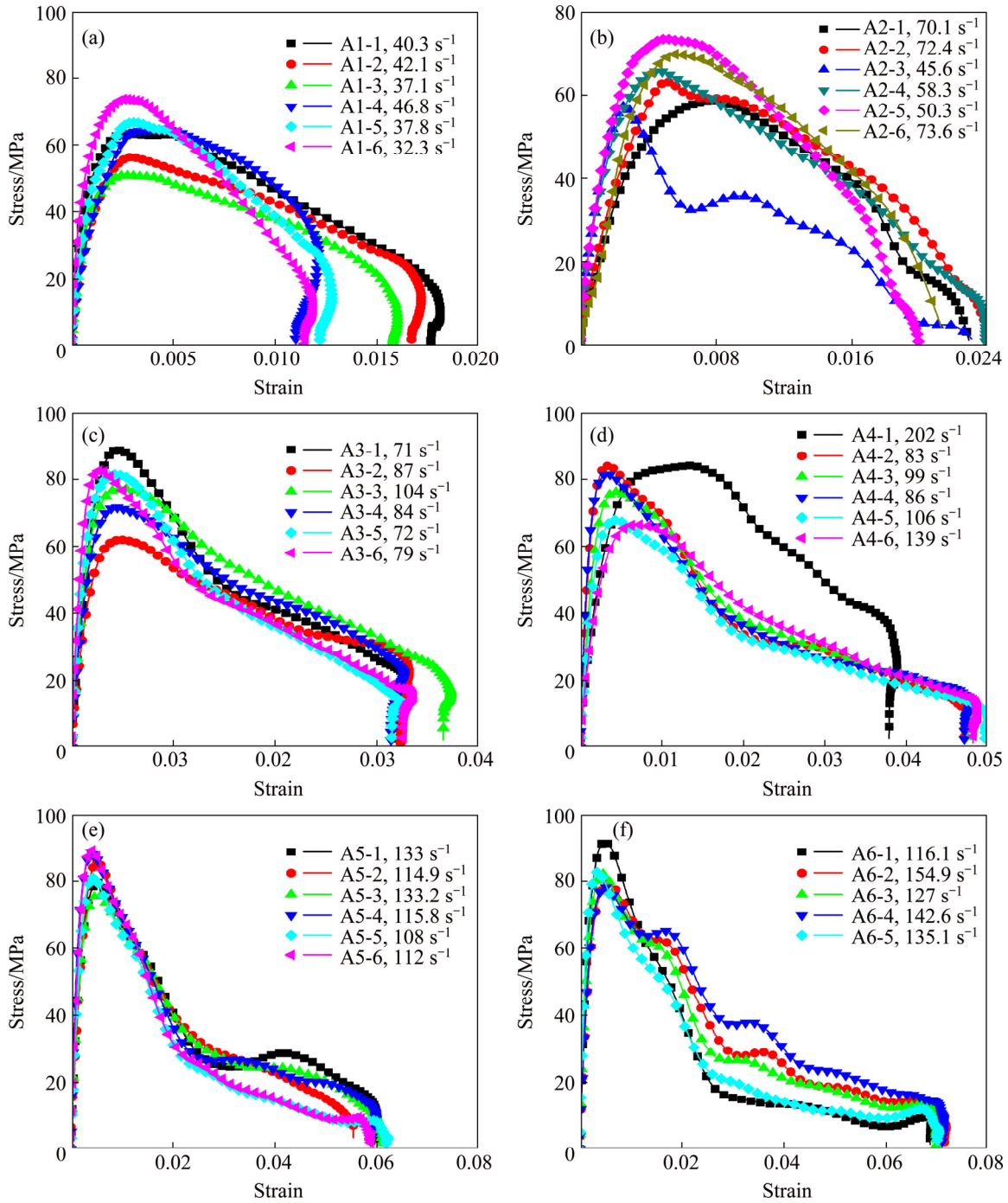

Fig. 2 Stress versus strain curves for mortar specimens with w/c=0.3: (a) A1; (b) A2; (c) A3; (d) A4; (e) A5; (f) A6

$$f = \frac{A}{B^{(w/c)}} \tag{4}$$

where f is the strength of concrete-like materials; A and B are constants for a given material, age and test conditions. Equation (4) and many other strength formulas [17−18] state the concrete strength is zero only when the water-to-cement ratio is infinitely high. Experience, however, does not support this: concrete strength can be negligible with high but still finite water-to-cement ratio. Although this distinction does not have practical significance while the water-to-cement ratio is within the practical range, it still can be taken care of as follows [19]:

$$f = A / B^{w/c} + C \tag{5}$$

where C is a third empirical parameter. When it is negative, the strength is negligible. When the water-to-cement ratio is very high, it is less than infinite. Thus, in the present work, the factors that affect the strength of cement mortar may be considered the water-to-cement ratio and the strain rate. Hence, a modified dynamic compressive strength and water-to-cement ratio between

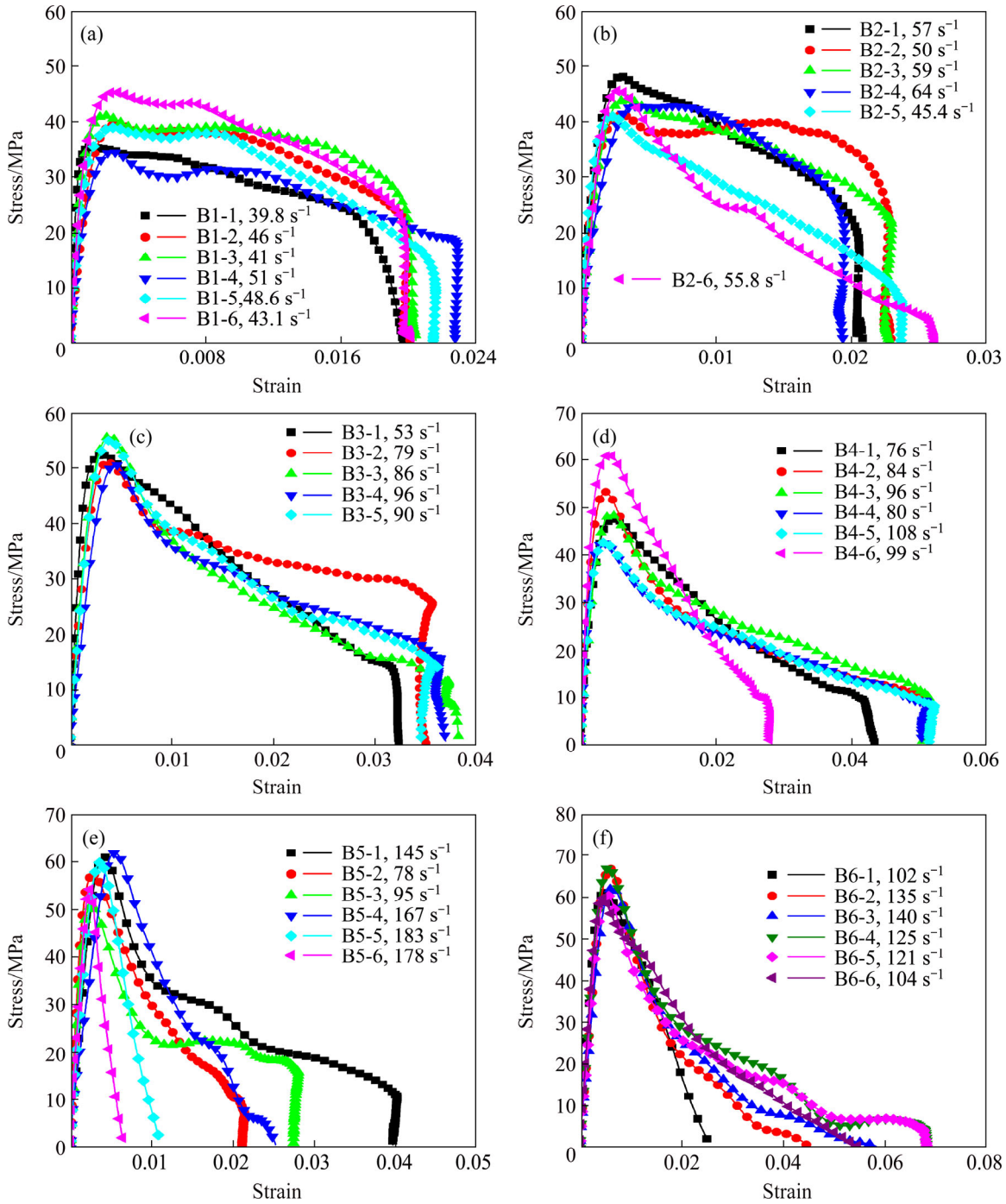

Fig. 3 Stress versus strain curves for mortar specimens with *w*/*c*=0.4: (a) B1; (b) B2; (c) B3; (d) B4; (e) B5; (f) B6

may be expressed as

$$\lg f = b_1 + b_2(w/c) + b_3(\dot{\varepsilon}) \tag{6}$$

where b_1, b_2 and b_3 are the constants of regression analysis. Analyzing the present strength results statistically by the principle of least squares, three normal equations involving the unknown regression parameters are obtained on solution, which yield the following equation:

$$\lg f = 2.059162 - 1.111(w/c) + 0.00135\dot{\varepsilon} \tag{7}$$

The value of the multiple correlation coefficient (R) has been obtained as 0.863 (Fig. 6). Expressed in exponential form, Eq. (7) can be written as

$$f = \frac{114.59}{129.91^{\alpha}} \tag{8}$$

where

$$\alpha = \frac{w}{c} - 0.1426\dot{\varepsilon} \tag{9}$$

3.4 Dynamic increase factor (DIF)

Figure 7 shows the dynamic increase factor (DIF) as

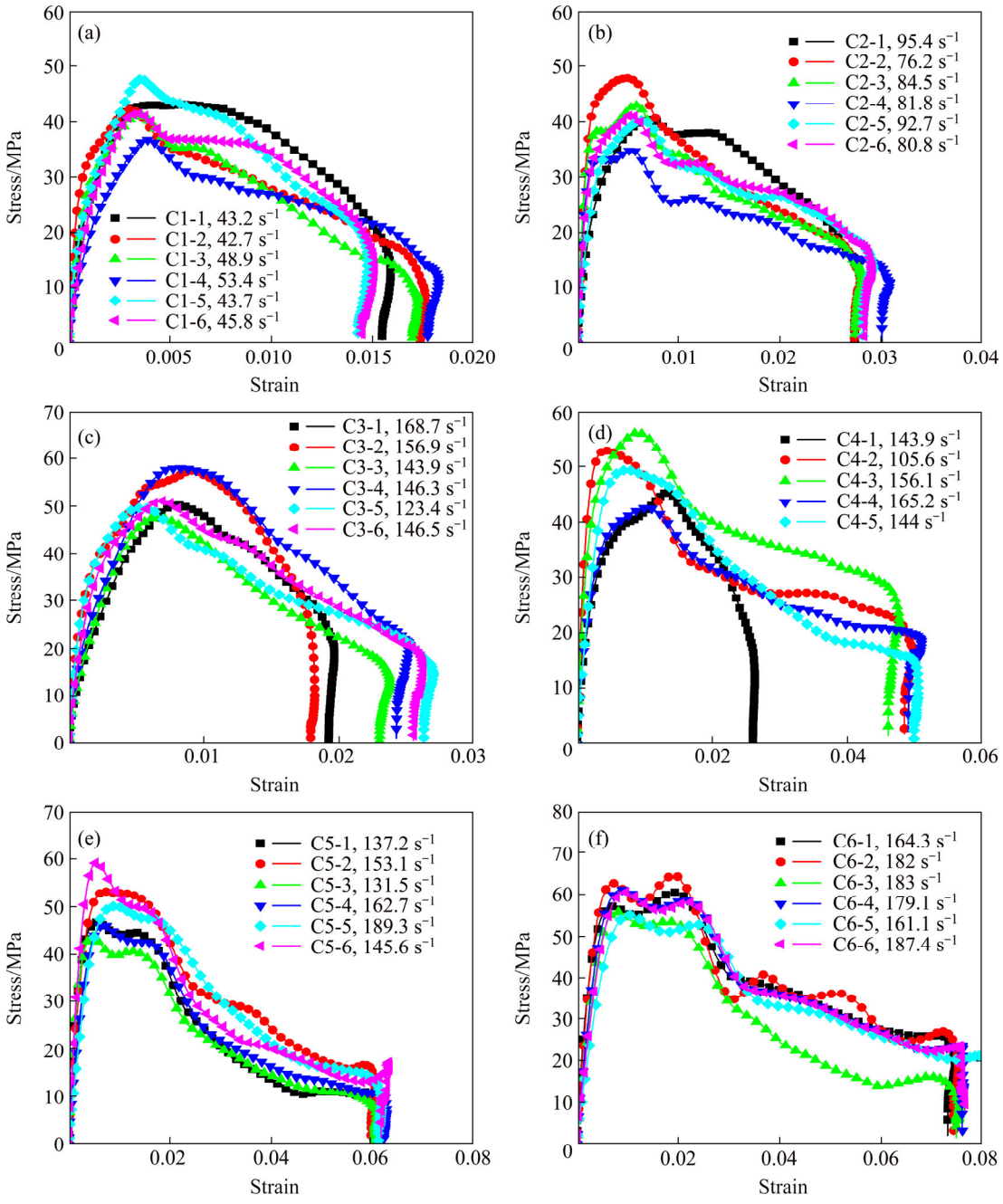

Fig. 4 Stress versus strain curves for mortar specimens with *w*/*c*=0.5: (a) C1; (b) C2; (c) C3; (d) C4; (e) C5; (f) C6

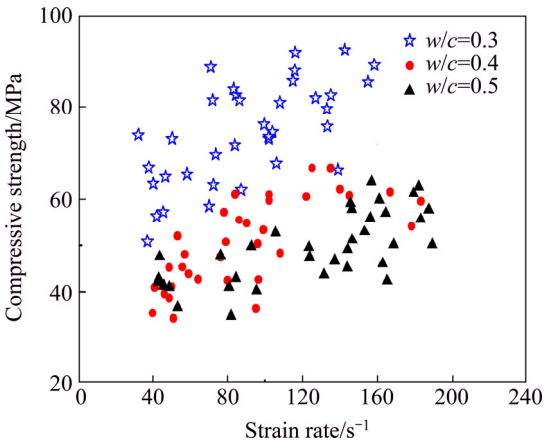

Fig. 5 Compressive strength versus strain rates for mortar

a function of strain rate. The DIFs are normalized by dividing the average compressive strength at static loading. Figure 10 indicates that with increase in strain rate, the DIF increases. However, this increase in DIF with increase in strain rate does not appear to be a function of the water-to-cement ratio.

The increase of the dynamic compressive strength in concrete was first observed by POPOVICS and UJHEYI [20] and it has been generally accepted that the uniaxial compressive strength of concrete material is strain-rate sensitive and the strength model of such materials should include strain-rate effects. A wide range of concrete and cement mortar with different quasi-static

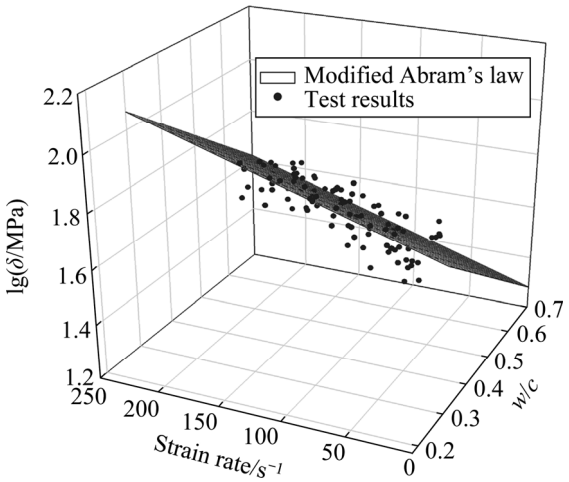

Fig. 6 Comparison of predicted results from modified Abram's law and test results

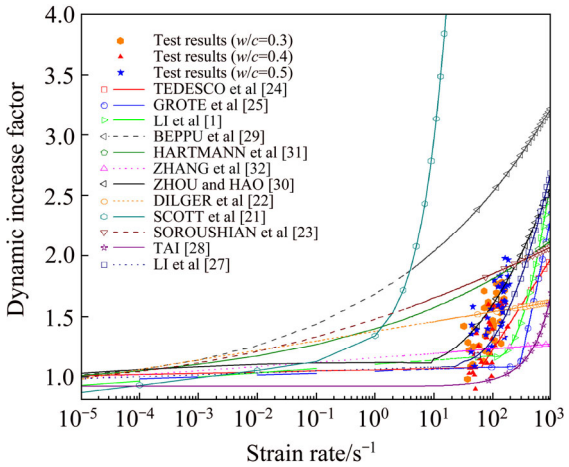

Fig. 7 DIF versus strain rates for mortar

strength have been tested in laboratories in order to quantify strain-rate effects [3], showing an obvious strength enhancement at strain-rates above a critical value between 10^1 and 10^2 s^{-1}.

SCOTT et al [21] studied the influence of strain rate on concrete using specimen of three different concrete qualities (compressive strength of 14, 22.4 and 35 MPa). An empirical relationship between the compressive DIF and strain rate was proposed:

$$\mathrm{DIF}=1.17+0.173\dot{\varepsilon}+0.06\lg\dot{\varepsilon} \tag{10}$$

According to DILGER et al [22], the DIF of plain concrete subjected to a strain rate can be expressed as

$$\mathrm{DIF}=1.38+0.08\lg\dot{\varepsilon} \tag{11}$$

The DIF equation, derived by SOROUSHIAN et al [23], has resulted from least-square curve fitting of a second-degree polynomial (in terms of $\lg\dot{\varepsilon}$) to the test results reported by different investigators. For DIF:

$$\mathrm{DIF}=1.48+0.160\lg\dot{\varepsilon}+0.0127(\lg\dot{\varepsilon})^2 \tag{12}$$

A series of SHPB tests have been conducted by TEDESCO et al [24] using SHPB for different concrete strengths, moisture and strain-rates around 10^2 s^{-1}. A DIF regression equation was suggested as follows:

$$\mathrm{DIF}=\begin{cases}0.00965\lg\dot{\varepsilon}+1.058\geq 1.0, & \dot{\varepsilon}\leq 63.1\ \mathrm{s}^{-1}\\ 0.758\lg\dot{\varepsilon}-0.289\leq 2.5, & \dot{\varepsilon}>63.1\ \mathrm{s}^{-1}\end{cases} \tag{13}$$

in which the transition point from a low strain-rate sensitivity to high strain rate sensitivity occurs at 63.1 s^{-1}.

GROTE et al [25] gave a formula to measure the DIF of mortar obtained by SHPB tests in the strain rate range of 250−1700 s^{-1}, i.e., with a transition strain rate of 266 s^{-1}. ZHANG et al [26] found that the formula is not continuous at the transition strain rate, when the DIF expression changes from a linear equation to a cubic equation. This discontinuity is overcome by a new data fitting expression using a linear and quadratic equations, as shown in Eq. (14).

$$\mathrm{DIF}=\begin{cases}1+0.00157(\lg\dot{\varepsilon}+3), & \dot{\varepsilon}\leq 266.0\ \mathrm{s}^{-1}\\ 0.383(\lg\dot{\varepsilon})^2+0.266\lg\dot{\varepsilon}-1.765, & \dot{\varepsilon}>266.0\ \mathrm{s}^{-1}\end{cases} \tag{14}$$

Based on the numerical results of mortar for three different slenderness ratios (i.e., length-to-diameter ratios), a relation between DIF and logarithm strain-rate was suggested by LI et al [1].

$$\mathrm{DIF}=\begin{cases}1+A_1(\lg\dot{\varepsilon}+A_2), & \dot{\varepsilon}\leq 10^2\ \mathrm{s}^{-1}\\ A_3(\lg\dot{\varepsilon})^2+A_4\lg\dot{\varepsilon}+A_5, & \dot{\varepsilon}>10^2\ \mathrm{s}^{-1}\end{cases} \tag{15}$$

where A_1=0.0344, A_2=3.0, A_3=1.729, A_4=−7.137, A_5=8.350 are determined by LI et al [1] using the least-squares method. They defined 10^{-4} s^{-1} as the quasi-static strain-rate, but the value of the DIF becomes unity when the strain-rate is 10^{-3} s^{-1}, which leads to a local drop at transition strain-rate. This abnormality can be eliminated by changing the values of A_1 and A_2 to 0.0258 and 4.0 [27].

Based on the results of the experimental program using Hopkinson bar apparatus, and through a rigorous calibration process, a new strain-rate dependent constitutive model was proposed by TAI [28]. This model is applicable to concrete strengths varying from 32 to 160 MPa with a strain-rate up to 1000 s^{-1}.

$$\mathrm{DIF}=0.9198\exp(0.00062\dot{\varepsilon}) \tag{16}$$

The constitutive equation to describe the dynamic increase factor (DIF) of compressive strength of concrete has been proposed by BEPPU et al [29] as shown in Eq. (17).

$$\mathrm{DIF}=(\dot{\varepsilon}/\dot{\varepsilon}_{\mathrm{s}})^{0.006\left[\lg(\dot{\varepsilon}/\dot{\varepsilon}_{\mathrm{s}})\right]^{1.05}} \tag{17}$$

Numerical simulations of concrete under compression at different strain rates were carried out by

ZHOU and HAO [30], the relative contribution of the inertial effect and the strain rate effect on compressive strength DIF is examined based on the numerical results. The DIF formula is shown as follows:

$$\mathrm{DIF}=\begin{cases}0.0225\lg\dot{\varepsilon}+1.12, & \dot{\varepsilon}\le 10\ s^{-1}\\ 0.2713(\lg\dot{\varepsilon})^2-0.3563\lg\dot{\varepsilon}+1.2275, & \dot{\varepsilon}\ge 10\ s^{-1}\end{cases} \tag{18}$$

In order to give a better fit to the underlying experimental data, new formulations for the dynamic strength increase have been developed and implemented by HARTMANN et al [31]. The DIF function for compressive loading is defined by

$$\mathrm{DIF}=0.5\cdot\left(\frac{\dot{\varepsilon}}{\dot{\varepsilon}_0}\right)^{0.13}+0.90 \quad \text{with} \quad \dot{\varepsilon}_0=1\ \mathrm{s}^{-1} \tag{19}$$

Similar to the last MC90, MC2010 [32] also contains a chapter on stress−strain rate effects, while the formulas of strain rate effect on concrete strength in MC2010 is simplified compared with that in MC90. In the code, within the strain rate range 3×10^{-5} $\mathrm{s}^{-1}<\dot{\varepsilon}<3\times10^{2}$ s^{-1}, the effect of strain rate on the compressive strength is shown as follows:

$$\mathrm{DIF}=\left(\frac{\dot{\varepsilon}}{\dot{\varepsilon}_\mathrm{s}}\right)^{0.014} \tag{20}$$

By plotting these relationships against the experimental results in this work (Fig. 10), the correspondence with the data obtained can then be appreciated. From Fig. 10, it can be found that the test results in this investigation agree well with the models of LI et al [27] and ZHOU and HAO [30]. From literature review and Fig. 10, it can be found that every empirical model agrees well with their respective experimental data and less well with the experimental data obtained by other authors, because each proposed equation was obtained by using a regression analysis to interpolate their own experimental data. Although all DIFs of empirical relations follow a similar trend, namely, DIF increases with the strain rate, scatters of the data from different authors are observed in Fig. 10. These scatters are attributed to variations in testing conditions such as equipment, specimen material (mortar or concrete), specimen size or differences in the moisture condition of the mixes.

3.5 Critical compressive strain

Critical compressive strain is defined as the strain when the stress reaches the peak. BISCHOFF and PERRY [3] summarized a wide range of concrete-like materials of various quasi-static strength and strain rates, showing that significant increases in critical compressive strain were sometimes observed during impact loading, although these increases were generally less than those observed for strength were. Figure 8 depicts a tendency that the critical compressive strain increases with the strain rate. By using data regression technique, the following equation could be obtained:

$$\varepsilon_\mathrm{c}=0.06\times[0.4119-0.4665\lg\dot{\varepsilon}+0.151(\lg\dot{\varepsilon})^2] \tag{21}$$

where ε_c denotes the critical compressive strain.

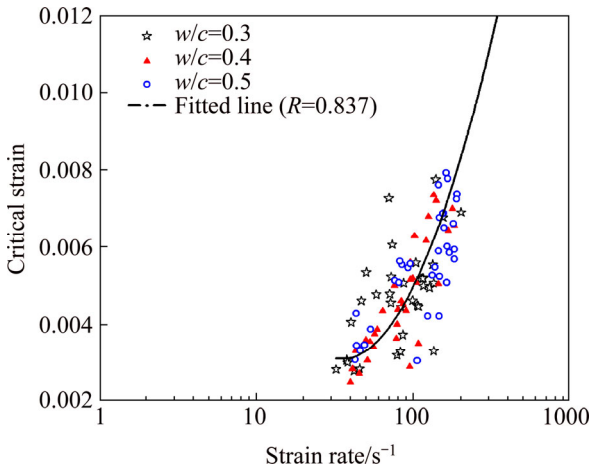

Fig. 8 Critical strain versus strain rates for mortar

At high strain rates, two alternative processes are likely for each growing crack: 1) the crack is forced to grow through a stiffer zone, or 2) the increased local stress intensity is relieved by the initiation or growth of other cracks in the vicinity that have no hindrance. The latter process causes a larger number of shorter length cracks, in place of a smaller number of longer cracks. Alternatively, during impact, cracks are likely to propagate in a straighter, more direct manner through zones of greater strength, such as sand grain, contributing also the higher stresses but less cracking. Eventually, for even further increases in stress, a stage can be reached at which impacted specimen will exhibit a greater degree of cracking. Both are allowing high strain capacity at peak stress.

4 Conclusions

1) The failure mode of mortar specimens is sensitive to the strain rate. At higher strain rate, cracks are larger in number and straighter, and the specimens produced a larger number of fragments at failure than at lower strain rates. The failure shows comparatively more violence at high strain rates. Mortar specimens with high water-to-cement ratio fail with comparatively less violence under the same strain rate.

2) A significant change in the stress-strain response of the materials with each order of magnitude increase in strain rate can be seen from test results. For mortar specimens, as the strain rate is increased, both the initial

slope and the peak stress increase, while the nonlinearity of the initial response decreases. The slope of the stress−strain curve after peak value reached is steeper than for the low water-cement mortar.

3) For the mortar in the range of high strain rates, the compressive strength increases with increasing strain rate. The dynamic increase factor (DIF) increases with the strain rate increasing, although it seems that in absolute value the increase of DIF with strain rate is independent of the water-to-cement ratio. The critical compressive strain increases with the strain rate.

4) It has long been known that concrete has a low tensile strength compared with its compressive strength. Since concrete is inherently weak in tension, it has been used as compressive member material in most concrete structures. However, it is difficult to isolate concrete members from dynamic tensile stresses. In future work, the tensile behavior of concrete under high strain rate will be studied.

References

[1] LI Q M, YE Z, Q, MA G W, REID S R. Influence of overall structural response on perforation of concrete targets [J]. International Journal of Impact Engineering, 2007, 34: 926−941.

[2] COTSOVOS D M, PAVLOVIC M N. Numerical investigation of concrete subjected to compressive impact loading. Part 2: Parametric investigation of factors affecting behaviour at high loading rates [J]. Computers and Structures, 2008, 86: 164−180.

[3] BISCHOFF P H, PERRY S H. Compressive behavior of concrete at high strain rates [J]. Materials and Structures, 1991, 24: 425−450.

[4] WANG Z L, WU L P, WANG J G. Experimental and numerical analysis on effect of fiber aspect ratio on mechanical properties of SRFC [J]. Construction and Building Materials, 2010, 24: 559−565.

[5] SUARIS W, SHAH S P. Properties of concrete subjected to impact [J]. Journal of Structural Engineering, 1983, 109: 1727−1741.

[6] HARSH S, SHEN Z, DARWIN D. Strain-rate sensitive behavior of cement Paste and mortar in compression [J]. ACI Materials Journal, 1990, 87: 508−516.

[7] WATSTEIN D. Effect of straining rate on the compressive strength and elastic properties of concrete [J]. ACI Journal Proceedings, 1952, 24: 729−744.

[8] DHIR R K, SANGHA C M. A study of the relationships between time, strength, deformation and fracture of plain concrete [J]. Magazine of Concrete Research, 1972, 24: 197−208.

[9] TEKALUR S A, SHUKA A, SADD M, LEE K W. Mechanical characterization of a bituminous mix under quasi-static and high strain rate loading [J]. Construction and Building Materials, 2009, 23: 1795−1802.

[10] ZHOU Z L, ZOU Y, LI X B, JIANG Y H. Stress evolution and failure process of Brazilian disc under impact [J]. Journal of Central South University, 2013, 20: 172−177.

[11] SUARIS W, SHAH S P. Rate-sensitive damage theory for brittle solids [J]. Journal of Engineering Mechanics, 1984, 110: 985−997.

[12] ATCHLEY B L, FURR H L. Strength and energy absorption capabilities of plain concrete under dynamic and static loadings [J]. ACI Journal Proceedings, 1967, 64: 745−756.

[13] ABRAMS D A. Effect of rate of application of load on the compressive strength of concrete [J]. ASTM Journal Proceedings, 1917, 17: 364−377.

[14] WU W, ZHANG W, MA G. Mechanical properties of coper slag reinforced concrete under dynamic compression [J]. Construction and Building Materials, 2010, 24: 910−917.

[15] TAI Y S. Uniaxial compression tests at various loading rates for reactive powder concrete [J]. Theoretical and Applied Fracture Mechanics, 2009, 52: 14−21.

[16] FREW D J, FORRESTAL M J, CHEN W. A split Hopkinson pressure bar technique to determine compressive stress-strain data for rock materials [J]. Experimental and Mechanics, 2001, 41: 40−46.

[17] GILKEY H J. Water-cement ratio versus strength—Another look [J]. ACI Journal Proceedings, 1960, 57: 1287−1312.

[18] NAGARAJ T S, BANU Z. Generation of Abrams's law [J]. Cement and Concrete Research, 1996, 26: 933−942.

[19] BHANJA S, SENGUPTA B. Modified water-cement ratio law for silica fume concretes [J]. Cement and Concrete Research, 2003, 33: 447−550.

[20] POPOVICS S, UJHEYI J. Contribution to the concrete strength versus water-cement ratio relationship [J]. Journal of Materials in Civil Engineering, 2008, 20: 459−463.

[21] SCOTT B D, PARK R, PRIESTLEY M J N. Stress−strain behavior of concrete confined by overlapping hoops at low and high strain rates [J]. ACI Journal Proceedings, 1982, 79: 13−27.

[22] DILGER W H, KOCH R, KOWALCZYK R. Ductility of plain and confined concrete under different strain rates [J]. ACI Journal Proceedings, 1984, 81: 73−81.

[23] SOROUSHIAN P, CHOI K B, ALHAMAD A. Dynamic constitutive behavior of concrete [J]. ACI Journal Proceedings, 1986, 83: 251−259.

[24] TEDESCO J W, POWELL J C, ROSS C A, HUGHES M L. A strain rate dependent concrete material model for ADINA [J]. Computers and Structures, 1997, 64: 1052−1067.

[25] GROTE D L, PARK S W, ZHOU M. Dynamic behavior of concrete at high strain rates and pressures: I. Experimental characterization [J]. International Journal of Impact Engineering, 2001, 25: 869−886.

[26] ZHANG M, LI Q M, HUANG F L, WU H J, LU Y B. Inertia-induced radial confinement in an elastic tubular specimen subjected to axial strain acceleration [J]. International Journal of Impact Engineering, 2010, 37: 459−464.

[27] LI Q M, LU Y B, MENG H. Further investigation on the dynamic compressive strength enhancement of concrete-like materials based on split Hopkinson pressure bar tests [J]. International Journal of Impact Engineering, 2009, 36: 1335−1345.

[28] TAI Y S. Uniaxial compressive tests at various loading rates for reactive powder concrete [J]. Theoretical and Applied Fracture Mechanics, 2009, 52: 14−21.

[29] BEPPU M, MIWA K, ITOH M, KATAYAMA M, OHNO T. Damage evaluation of concrete plates by high-velocity impact [J]. International Journal Impact Engineering, 2008, 35: 1419−1426.

[30] ZHOU X Q, HAO H. Modelling of compressive behaviour of concrete-like materials at high strain rate [J]. International Journal of Solid Structures, 2008, 45: 4648−4661.

[31] HARTMANN T, PIETZSCH A, GEBBEKEN N. A hydrocode material model for concrete [J]. International Journal of Protective Structures, 2010, 1: 443−468.

[32] ZHANG X, RUIZ G, YU R C, POVEDA E, PORRAS R. Rate effect on the mechanical properties of eight types of high strength concrete and comparison with FIB MC2010 [J]. Construction and Building Materials, 2012, 30: 301−308.

(Edited by YANG Hua)